Indian Geotechnical Journal, 33 (4), 2003

Performance of a Thermodynamic Constitutive Model for Granular Materials

Aniruddha Sengupta*

Introduction

In this paper, a thermodynamic material model based on the universal laws of thermodynamics has been utilized to predict the mechanical behaviour of frictional materials like, sand and cemented sand.

A large number of constitutive models for granular materials exist today. Lade's model (Lade, 1977), Prevost's multiple yield surface model (Prevost, 1978), Sandler and Baladi's cap model (Sandler, 1976), Dafalias's bounding surface model (Dafalias, 1983), Mroz's model (Mroz, 1984), Desai's Hierarchical Model (Desai, 1987), Modified Cam-Clay model (Roscoe, 1967), and Duncan and Chang's Hyperbolic model (Duncan, 1970) are some of the well known and well established soil models besides the classical plasticity models like, Von Mises model and Mohr-Coulomb model. It is not within the scope of this paper to discuss the superiority and advantages of these different models over each other. The readers may refer to the proceedings of the international benchmark conferences (Yong and Ko, 1980; Saada, 1987 and Arulanandan, 1993) for the comparative performances of these different models.

One of the drawbacks of the above plasticity models is that they are all based on Drucker's postulate or Il'yushin's postulate and the principle of maximum work, which essentially require that the mechanical work done should be always positive. But Mandel (Mandel, 1964) has shown that granular (frictional) materials like, soils, do not obey Drucker's stability postulates (Drucker, 1956, 1959) and may do some negative work upon a stress reversal if the plastic strain is not zero along a cyclic stress path.

* Assistant Professor, Indian Institute of Technology, Kharagpur – 721302, India.
E-mail: Sengupta@civil.iitkgp.ernet.in

Thus, Drucker's postulate is a sufficient condition, but not a necessary one. In granular materials, negative plastic work must be done upon a stress reversal if the plastic strain is not zero, that is, the plastic strain increment is in the opposite direction from the stress. More recently, Lade (Lade, 1987) has also proved experimentally the same, that is, laboratory tests on granular materials were reported to be stable yet violated Drucker's postulate both in large and in the small. Another disadvantage of the existing plasticity models are that they all require knowledge regarding the shape of the yield surface(s) for the particular material a priori. Also the definition of the yield surfaces varies from model to model and thus far to the confusion of the users, a large number of yield surfaces have been proposed.

The thermodynamic theory under consideration, being based on a much more fundamental principle of second law of thermodynamics, unlike existing plasticity models, allows negative mechanical work done during stress reversal as long as the total entropy of the system remains positive. Also the thermodynamic model does not require any a priori definition of the yield surface. Yet various plastic models are shown (Sengupta, 1989) to be constitutive subsets of this theory and the phenomenon of yielding is a consequence of a particular definition of the intrinsic time measure and appears in a posteriori fashion. The kinematic hardening, isotropic hardening and their combinations may be derived directly from the thermodynamic theory. When the general theory degenerates to elastic-plastic theories, it does obey Drucker's postulates and show closure of hysteresis loop.

The thermodynamic theory under consideration was originally proposed by Valanis and Peters (1988). Present paper focuses on the ability of the model to degenerate to a Mohr-Coulomb type of theory showing prominent yield surface and dilatant behaviour during shearing. The model has been used to predict the mechanical response of a Hostun sand and a cemented sand along different stress paths including circular and cyclic stress paths for which the model is not calibrated. Present paper concentrates only on the performance of the model. Actual determination of the material parameters and calibration of the model for the above two soils are shown elsewhere (Sengupta and Saxena, 1991).

The Thermodynamic Theory

The deviatoric and hydrostatic stresses in the thermodynamic theory are given by

$$\tilde{s} = \int_0^{Z_D} \rho(Z_D - Z)\frac{\partial \tilde{e}^p}{\partial Z} dZ \qquad (1)$$

and

$$\sigma = \frac{\sigma_{kk}}{3} = \int_0^{Z_H} \phi(Z_H - Z)\frac{\partial \varepsilon^p}{\partial Z}dZ + \int_0^{Z_H} \Gamma(Z_H - Z)\tilde{s}\cdot\frac{\partial \tilde{e}^p}{\partial Z}dZ \quad (2)$$

where,
$$\rho(Z_D) = \sum_{r=1}^{N} A_r e^{-\alpha_r Z_D} \quad (3)$$

$$\phi(Z_H) = \sum_{r=1}^{N} B_r e^{-\beta_r Z_H} \quad (4)$$

$$\Gamma(Z_H) = \sum_{r=1}^{N} \beta_r \frac{b_{21}^{(r)}}{f_H} e^{-\beta_r Z_H} \quad (5)$$

A_r, α_r, B_r, β_r are material parameters. A_r and α_r are deviatoric components of the internal variables. B_r and β_r are the hydrostatic components of the internal variables. e^p and ε^p are the plastic deviatoric strain tensor and plastic hydrostatic strain, respectively. $b_{21}^{(r)}$ are the resistance tensors. r is the number of mechanisms. Z is the intrinsic time scale and, Z_D and Z_H are the deviatoric and hydrostatic components of Z. dZ, dZ_D and dZ_H are defined as

$$dZ^2 = dZ_D^2 + k^2\, dZ_H^2 \quad (6)$$

with,
$$dZ_D = \frac{dZ}{f_D} = \left\| d\tilde{e}^p \right\| \quad (7)$$

$$dZ_H = \frac{dZ}{k\, f_H} = \left| d\varepsilon^p \right| \quad (8)$$

where

k = coupling term,

f_D = deviatoric hardening functions,

f_H = hydrostatic hardening functions,

$\left\| d\tilde{e}^p \right\|$ = denotes norm of the incremental plastic deviatoric strain tensor, and

$\left| d\varepsilon^p \right|$ = represents the absolute value of plastic hydrostatic strain.

A complete derivation of the above equations from the principles of thermodynamics is shown by Sengupta and Saxena (1991). If it is assumed that the effect of the deviatoric plastic work rate is distributed uniformly among all the hydrostatic mechanisms, then it is possible to have

$$b_{21}^{(r)} = b_{21}^{0} \tag{9}$$

and

$$\Gamma(Z_H) = b_{21}^{0}\,\phi(Z_H) \tag{10}$$

It is often difficult to work with the equations in the integral forms. The Eqns.(1) and (2) may be conveniently expressed in differential forms as

$$(\tilde{s}-\tilde{r}) = \rho_0 f_D \frac{d\tilde{e}^P}{dZ} \tag{11}$$

and

$$(\sigma - r') = \phi_0 \frac{d\varepsilon^P}{dZ_H} + \Gamma_0 \tilde{s}\cdot\frac{d\tilde{e}^P}{dZ} - \frac{1}{\phi_0}\frac{d\sigma}{dZ_H} \tag{12}$$

where $$\tilde{r} = \int_0^{Z_D} \rho_1(Z_0 - Z)\frac{\partial \tilde{e}^P}{\partial Z}dZ, \text{ and} \tag{13}$$

$$r' = \int_0^{Z_H} \phi_1(Z_H - Z)\frac{\partial \varepsilon^P}{\partial Z}dZ + \int_0^{Z_H} \Gamma_1(Z_H - Z)\cdot\tilde{s}\cdot\frac{\partial \tilde{e}^P}{\partial Z}dZ \tag{14}$$

ϕ_0, ρ_0, Γ_0 are material parameters and ϕ_1, ρ_1 and Γ_1 are functions like ϕ, ρ and Γ respectively. Thus the equation for the yield surface is given by

$$\|\tilde{s}-\tilde{r}\|^2 + \left(\frac{\rho_0 f_D}{k\phi_0 f_u}\right)^2\left[(\sigma - r') - \frac{\Gamma_0}{\rho_0 f_D}\tilde{s}\cdot(\tilde{s}-\tilde{r})\right]^2 - \rho_0^2 f_D^2 = 0 \tag{15}$$

Above equation describes a yield behaviour that includes both kinematic and isotropic hardening. If f_D and f_H are constant, the behaviour is purely kinematic. For incompressible material, like metals, where $\phi_0 f_H \to \infty$, the deviatoric projection of the yield surface is circular with radius $\rho_0 f_D$ showing Von Mises type of yield surface. While for compressible materials like soils and concrete, where $\Gamma \neq 0$, the projection in the deviatoric plane is non-circular.

The Mohr-Coulomb type of behaviour may be accomplished by assuming that the hydrostatic response may be represented by the summation of a series containing only a single exponential term, thus

$$\phi(Z_H) = \phi_0 \delta(Z_H) \tag{16}$$

and

$$\Gamma(Z_H) = \Gamma_0 f_H \delta(Z_H) \tag{17}$$

where, δ = Dirac-Delta function

$$\Gamma_0 = \sum_{r=1}^{N} b_{21}^{0\ r} \tag{18}$$

For this particular case, the hydrostatic stress may be expressed as:

$$\sigma = \frac{\sigma_{\kappa\kappa}}{3} = \phi_0 f_H k \frac{d\varepsilon^P}{dZ} + \Gamma_0 \tilde{s} \cdot \frac{d\tilde{e}^P}{dZ} - \frac{1}{\phi_0} \frac{d\sigma}{dZ_H} \tag{19}$$

For purely hydrostatic condition $\left(\tilde{s} = 0,\ \tilde{e}^P = 0\right)$,

$$\sigma = \varphi_0 \left(\varepsilon^P\right) \tag{20}$$

If it is assumed that the material is isotropic, the deviatoric stress may be expressed as

$$\tilde{s} = \rho_0 f_D \frac{d\tilde{e}^P}{dZ} \tag{21}$$

For a Mohr-Coulomb type of behaviour, the deviatoric hardening parameter should be expressed in the following form

$$f_D = \delta_0 + \eta\sigma \tag{22}$$

where, δ_0 and η are material parameters and σ is the mean stress.

It can be shown that under constant hydrostatic stress condition (Valanis and Peters, 1988), deviatoric and hydrostatic plastic strains may be related by the following equation

$$k\frac{d\varepsilon^{p}}{d\bar{e}^{p}} = \frac{1-\Gamma_0^2 S^{*2}}{f_H \Gamma_0 S^{*} + \sqrt{f_H^2 + \Gamma_0^2 s^{*2} - 1}} \tag{23}$$

with

$$f_H = (1-\varphi_1)e^{\beta \bar{e}^{p}} + \varphi_1 \tag{24}$$

and

$$S^{*} = \frac{\tilde{s}}{\sigma} \tag{25}$$

In the above equations, Γ_0 is a coupling term, which relates the shear-induced volume change to the deviatoric plastic work. β and φ_1 are material parameters and ϕ_0 is any suitable large number needed for the closure of hysteresis loops under hydrostatic loading cycles.

Performance of the Model

The major motivation of this research effort is to investigate the performance of a theory which is based on second law of thermodynamics instead of over restrictive postulates, in modeling elasto-plastic material behaviour like frictional-dilatant behaviour and mean stress dependency. The performance of the thermodynamic model was studied by comparing the laboratory test results and the corresponding model predictions of a dry sand and a cemented sand. The laboratory tests were performed along different stress paths for which the model was not calibrated. Table 1 summarizes all the stress paths that the model was subjected to in order to evaluate its performance for a dry sand and a cemented sand.

For Dry Sand

The dry sand used for testing the performance of the thermodynamic model is known as Hostun sand. Hostun sand is a quarry sand available commercially through SIKA Ltd. The properties of the sand are as follows:

Percentage of sand	:	99.5%
Grain Density	:	2.667
Maximum Density	:	1.66 g/cc
Minimum Density	:	1.35 g/cc

A detailed description of the sand may be obtained from Saada (1987).

TABLE 1 : Performance of the Model along Different Stress Paths

Material Tested	Testing Device	Stress Path	Confining Pressure	Performance of the Model
Dense Hostun Sand Density = 1.65 gm/cc	Hollow Cylinder	Consolidated Drained Compression, b = 0	203 kPa	Calibration test
	Cubical Device	Consolidated Drained Compression, b = .286	500 kPa	Good
	Cubical Device	Consolidated Drained Compression, b = .666	500 kPa	Good
	Hollow Cylinder	Cyclic Torsion Test, b = variable	500 kPa	Not Good
	Hollow Cylinder	Monotonic Torsion Test	500 kPa	Good
	Cubical Device	Circular Stress Path, b = variable	500 kPa	Not Good
Cemented Sand Density = 1.65 gm/cc DR = 80%	Conventional Triaxial	Consolidated Drained Compression, b = 0	49 kPa	Good
			245 kPa	Calibration test
			490 kPa	Good

For the material parameter determination of Hostun sand, the data from a single consolidated drained test (b = 0) performed in a hollow cylinder device under an initial spherical stress of 203 kPa were utilized. No hydrostatic test was used for material parameter determination due to the fact that they had been conducted at low pressures and thus would not represent the yielding behaviour of the sand. Based on the past knowledge of Hostun sand and using the fact that the predictions do not require an accurate response to changes to σ, the function φ_0 in Eqn.20 was assumed to be constant. For a frictional material following Mohr-Coulomb law, the functional form of the deviatoric hardening parameter is given by Eqn.22. It physically represents the failure envelope during shearing under constant hydrostatic stress, σ. For pure sand, $\delta_0 = 0$ and η is chosen in such a way that $f_D = 1$ at some convenient mean stress level. To have a yield surface type of theory, ϕ_0 in Eqn.19 should be given a suitable large value such that

$$\phi_0 = \sum_{r=1}^{N} B_r = \infty \tag{26}$$

The deviatoric components {three mechanisms (N = 3) was assumed for Hostun sand} of the internal variables were determined by curve fitting subjected to the following constraints

$$A = \sum_{r=1}^{N} A_r = \infty \tag{27}$$

and

$$\sum_{r=1}^{N} \frac{A_r}{\alpha} = \sigma_Y \tag{28}$$

where, σ_Y is the yield stress.

The detailed procedure for the determination of material parameters for Hostun sand is given in Sengupta and Saxena (1991). The material parameters for the Hostun sand are given in Table 2.

To check the fitting procedure, the stress-strain and the volumetric response of the Hostun sand predicted by the model have been compared with the hollow cylinder test data for which the model has been calibrated. Close fits between the test data and model predictions, as shown in Fig.1, depict the accuracy of the whole fitting procedure.

TABLE 2 : Material Parameters for Hostun Sand

Elastic Parameters		
Bulk Modulus	K (kPa)	225000.0
Shear Modulus,	G (kPa)	100000.0
Unit Weight	γ (kN/m^3)	16.9
Dilatancy Parameters	k	0.741
	Γ_0	1.026
Deviatoric Hardening Parameters	ϕ (degree)	39.0
	η	0.002
	δ_0	0.0000001
Hydrostatic Hardening Parameters	φ_1	0.817
	φ_0	1018.9
	ϕ_0	1750000.0
Deviatoric Internal Variables	A_1	16480.0
	α_1	83.794
	A_2	52000.0
	α_2	403.2
	A_3	250000.0
	α_3	773.55

The performance of the model was evaluated by comparing the model predictions with the corresponding test results performed along five completely different laboratory generated stress paths for which the model was not calibrated. Fig.2 shows the model predictions for the case of a true triaxial (cubical) test performed at a confining pressure of 500 kPa and with b = 0.286. The stress ratio, b is defined as

$$b = \frac{\sigma_2 - \sigma_3}{\sigma_1 - \sigma_3} \quad \text{for } \sigma_1 > \sigma_2 > \sigma_3 \tag{29}$$

Figure 3 shows the model performance for the case of a true triaxial test performed at a confining pressure of 500 kPa and with stress ratio, b = 0.666.

The terms, SD2, S1 and ID2 used in the figures are stress and strain invariants and defined as

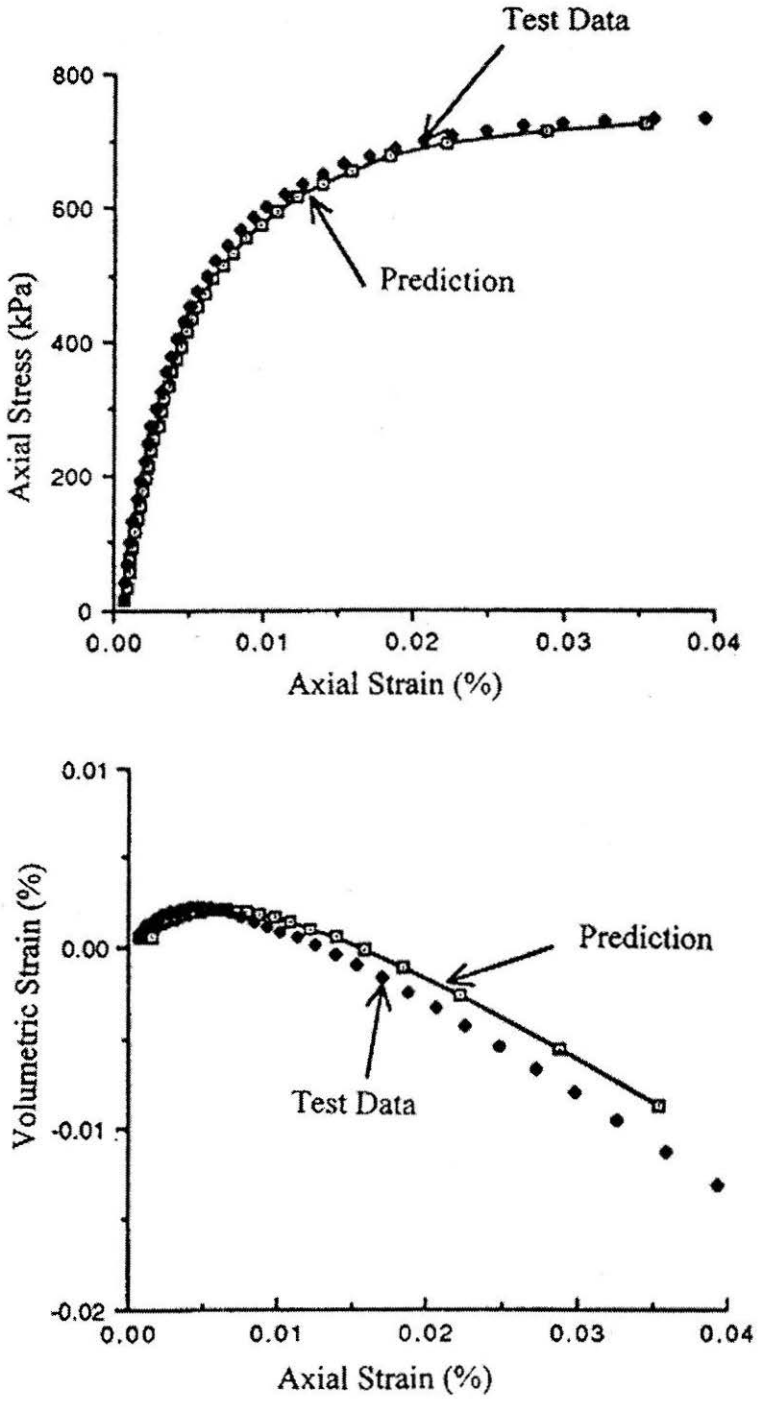

FIGURE 1 : Model Performance for Hollow Cylinder Test at 203 kPa

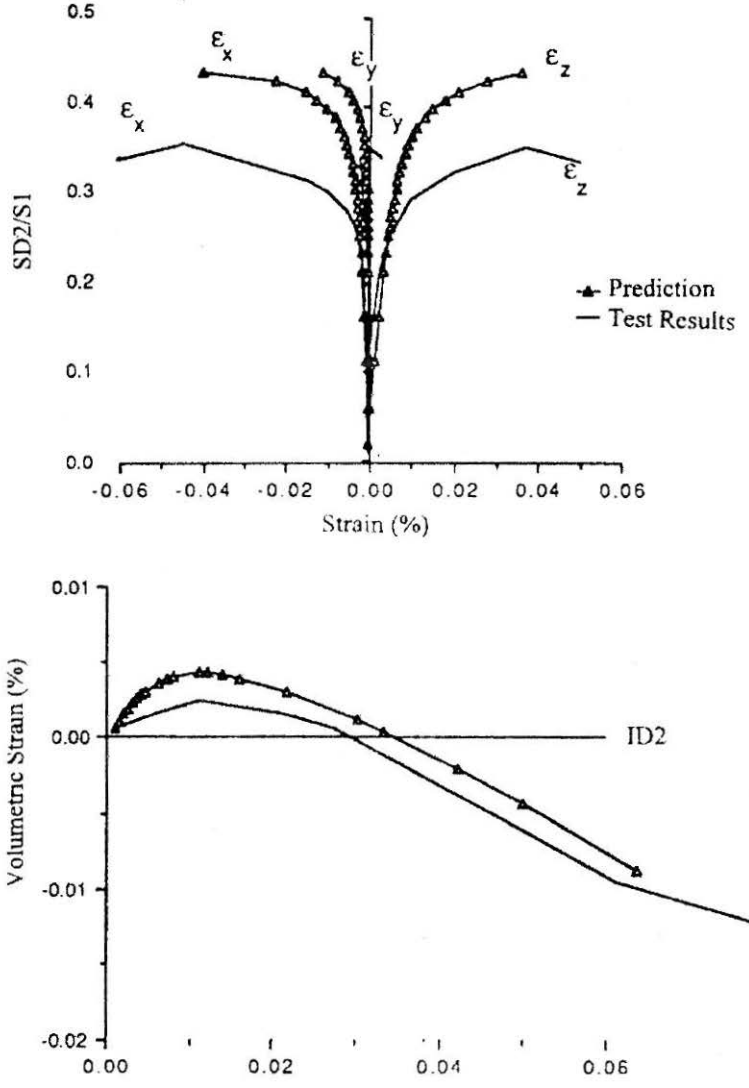

FIGURE 2 : Predictions for Cubical Test with b = 0.286

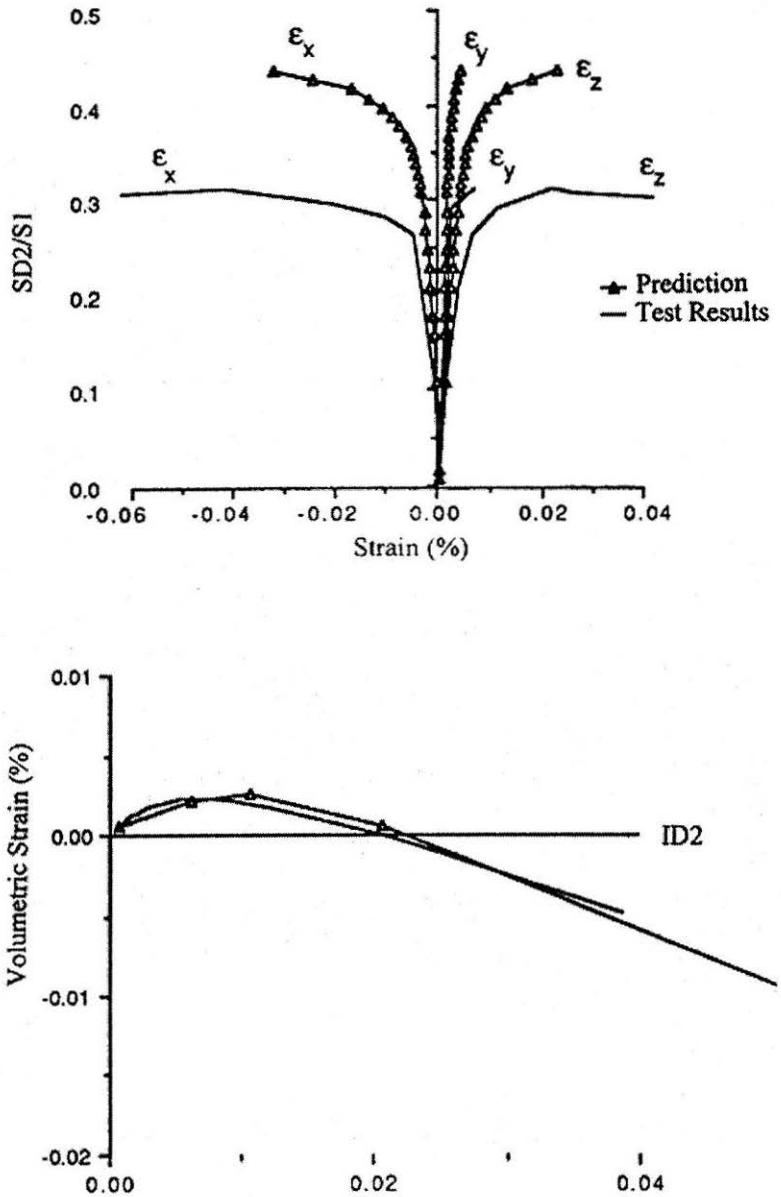

FIGURE 3 : Predictions for Cubical Test with b = 0.666

$$SD2 = \sqrt{\frac{1}{3}\left[(\sigma_X - \sigma_Y)^2 + (\sigma_Y - \sigma_X)^2 + (\sigma_X - \sigma_Z)^2\right]} \tag{30}$$

$$SI = \frac{(\sigma_X + \sigma_Y + \sigma_Z)}{3} \tag{31}$$

$$ID2 = \sqrt{\frac{1}{3}\left[(\varepsilon_X - \sigma_Y)^2 + (\varepsilon_Y - \sigma_X)^2 + (\varepsilon_X - \sigma_Z)^2\right]} \tag{32}$$

Model predictions in both the above cases show slightly stiff stress-strain responses. However the volume change responses were found to be very good. The stiffer stress-strain response of the model might be due to the fact that hollow cylinder tests typically show stiffer response than cubical triaxial tests. Thus the slight over estimation of stiffness could have been avoided if cubical test results were used instead of hollow cylinder test results for calibrating the model. The overall model performances were found to be quite good for both the cases considering the fact that the boundary/loading conditions and sample sizes were quite different between a hollow cylinder test and cubical test.

Figures 4, 5 and 6 show the performance of the model in simulating a cyclic torsion test (b = variable, β = variable) performed in a hollow cylinder device. The test parameter, β, is defined as follows:

$$\tan(2\beta) = \frac{2\gamma_{\theta Z}}{(\sigma_Z - \sigma_\theta)} \tag{33}$$

This test was conducted in three stages. In the first stage, the axial stress was increased to 520 kPa and it was maintained constant throughout the experiment. In the second stage, the sand was subjected to 5 cycles of sinusoidally varying shear stresses with an amplitude of 133 kPa. This portion of the test is referred to as cyclic torsion test. In the third stage, the shear stress was monotonically increased to failure. This last portion of the test is referred to as monotonic torsion test. Figures 4 and 5 compare the model performance with the test results for the second stage (cyclic portion) of the test. The model predictions show stiffer behaviour. The volume change response, shown in Fig.5, was found to be dilative. The results indicate a large kinematic surface during the cyclic part. The yield surface was found to be swinging with the progress of loading. Above two anomalies result in large volumetric strains predicted by the model and suggest the need for including the third invariant of stress (J_{3D}) in the model formulations, which is found to be controlling in this stress path. The fact is that, most of the

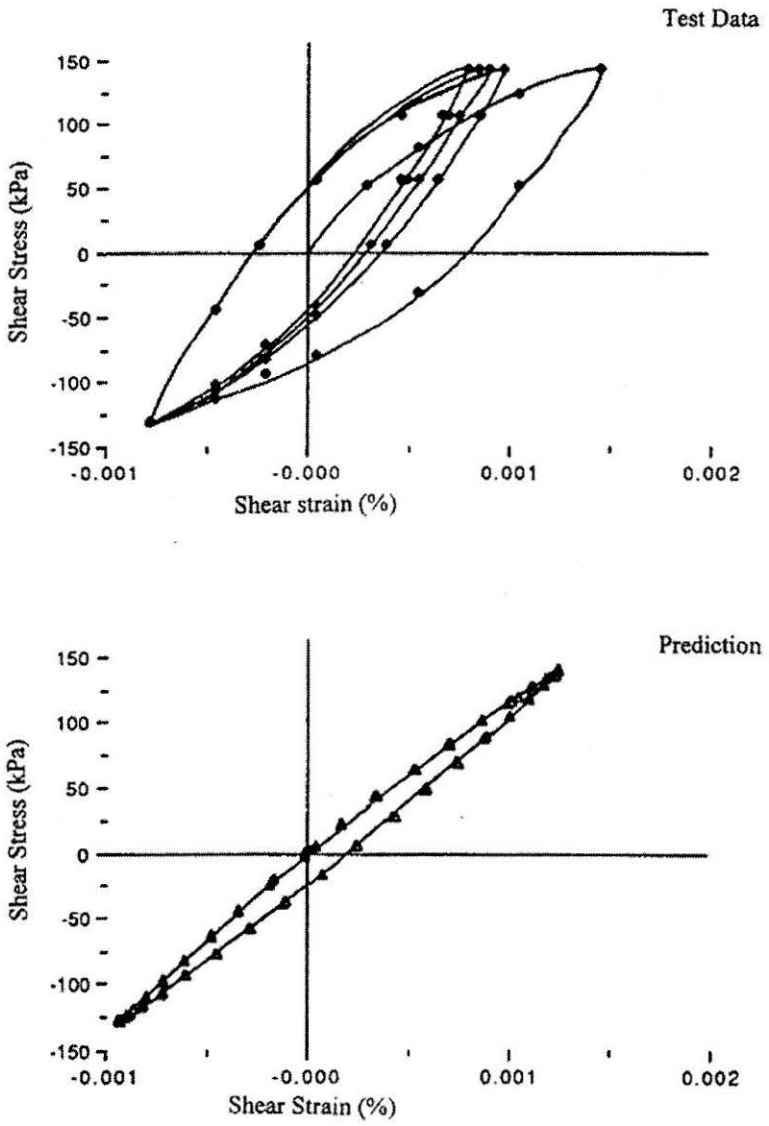

FIGURE 4 : Prediction for Hollow Cylinder Test along Cyclic Torsion Stress Path (b = variable)

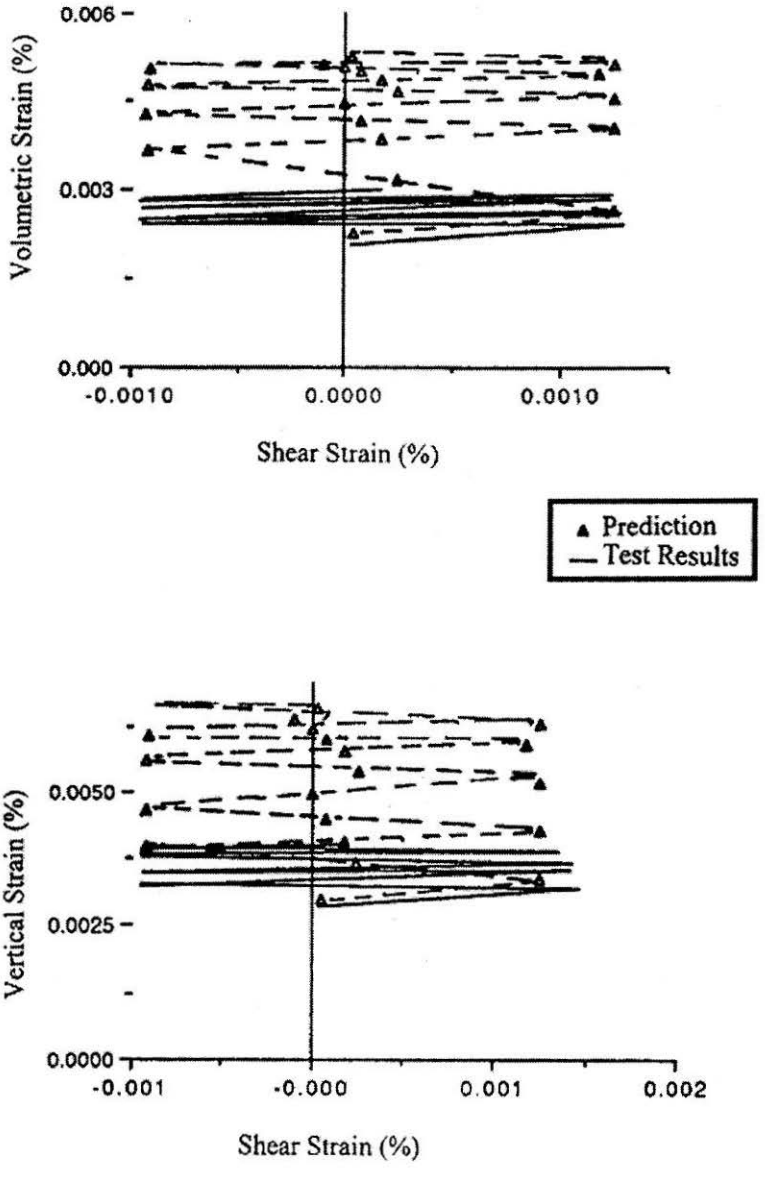

FIGURE 5 : Prediction for Hollow Cylinder Test along Cyclic Torsional Stress Path (b = variable)

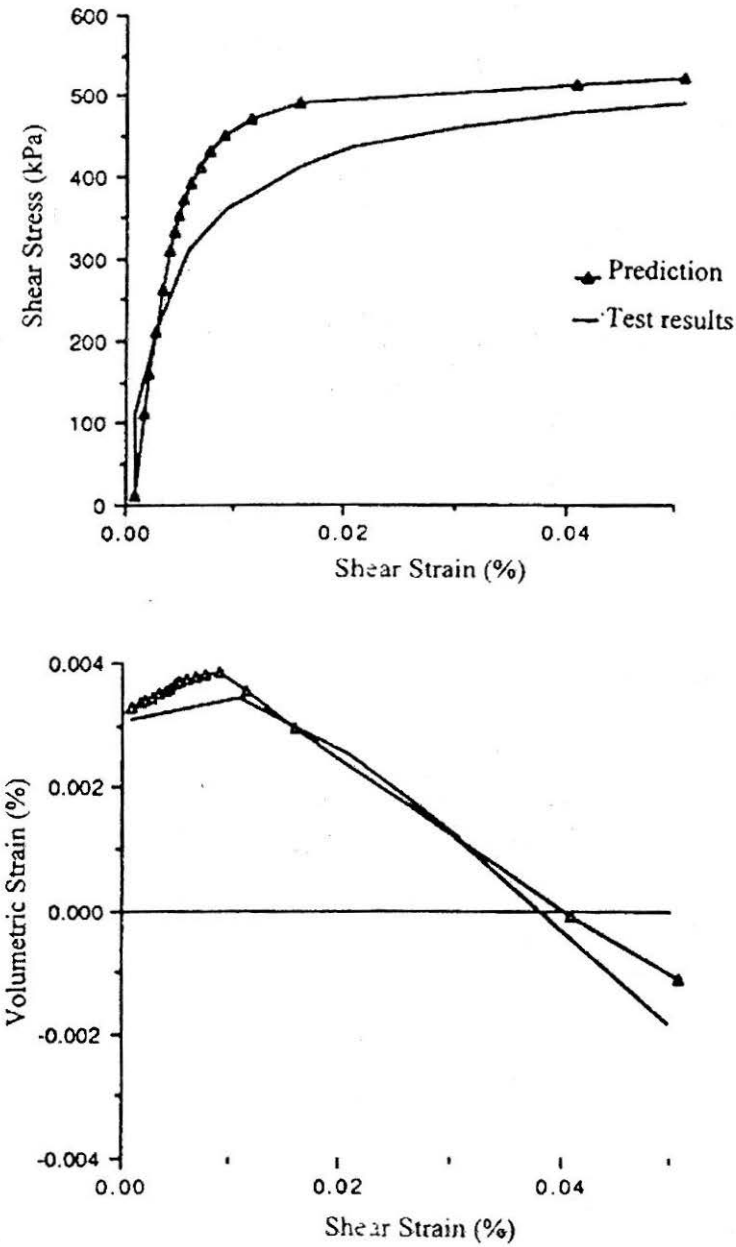

FIGURE 6 : Prediction for the Hollow Cylinder Test along Monotonic Torsional Stress Path

plasticity models (Saada, 1987) including the present thermodynamic model, which do not have third invariant of stresses included in their formulation will not perform well in this stress path. At present, research is underway to find a way to include the third invariant of deviatoric stresses through the deviatoric hardening parameters of the thermodynamic model.

The model prediction for the third stage of the test (shown in Fig.6), that is for the monotonic torsion test, was found to be quite close to the laboratory results because here the effect of J_{3D} is minimal again.

Figures 7 and 8 compare the model predictions with the corresponding test results for a test performed along a circular stress path in a cubical (true triaxial) device. During the initial stage of this test, the vertical stress, σ_z, was increased and horizontal stresses, σ_y and σ_x, were decreased so that the mean stress remained constant at 500 kPa and the second invariant of stresses, SD2, equal to 420 kPa. In the second stage, the stresses were varied sinusoidally so that the mean and deviatoric stresses remained constant. When plotted on the π-plane, the stress path projects as a circle. Figure 7 shows the variation of the strains (ε_v, ε_z, ε_y and ε_x) with the stress phase angle (Φ_σ). Stress phase angles varying from $-120°$ to $240°$ represent the first cycle. Stress phase angle varying from $240°$ to $600°$ represent the second cycle. Figure 8 shows the model predictions in strain π-plane. As apparent from both the figures, the model exhibited stiffer response along the circular stress path. The apparent mismatch between the model predictions and test results is again due to the absence of third invariant of stress in the present formulations of the model. Actually, the model predictions as shown in Figs.7 and 8 are quite reasonable because this is a very difficult stress path and most of the existing models fail to predict accurately in this particular stress path (Saada, 1987).

From the above comparisons it may be concluded that the thermodynamic model has the ability to predict the mechanical behaviour of a sand in different stress paths for which it is not calibrated. The model responses are in general stiff, which might be due to the fact that the effect of the third invariant of stresses is not included in the present formulation of the thermodynamic model and the hollow test results, which are used for model calibration, are themselves stiffer as compared to cubical test results.

For Cemented Sand

The laboratory test results used in this study for demonstrating the performance of the thermodynamic model in case of cemented sand are taken from Avramidis (1985). The cemented sand considered here has 2% cement content (CC) and 80% relative density (DR). The cemented sand was cured for 15 days before testing. The elastic properties like, Young's modulus,

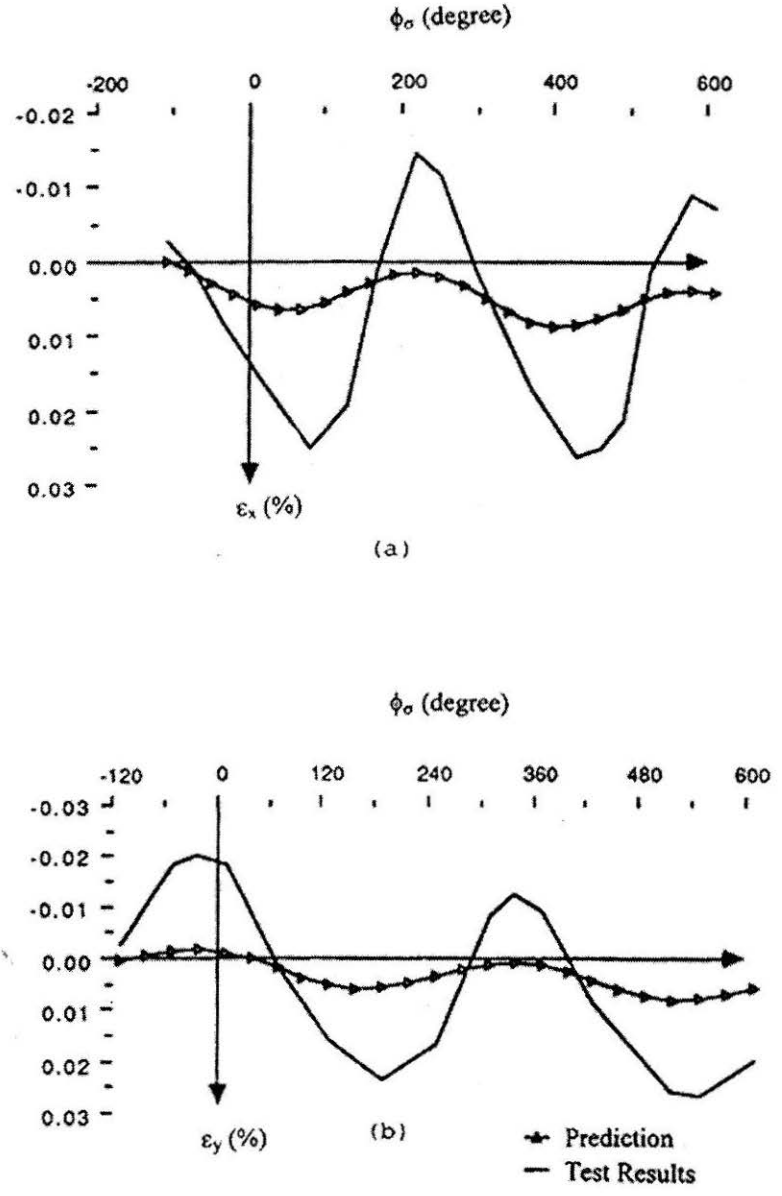

FIGURE 7 : Performance for the Cubical Test along Circular Stress Path (b = variable)

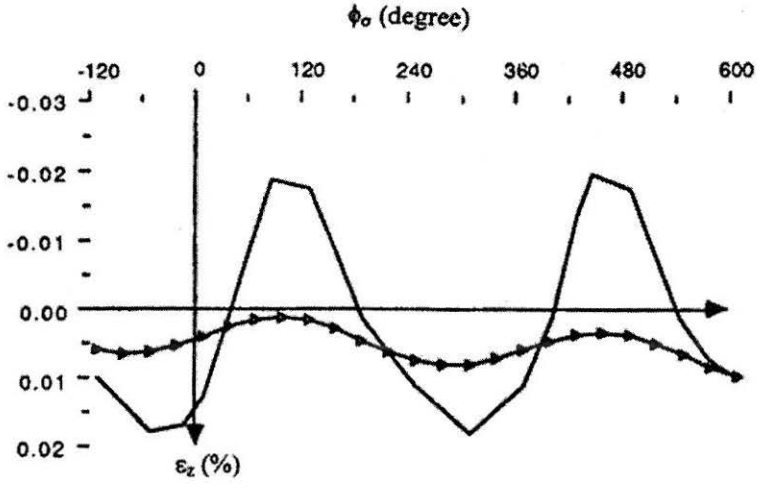

(c)

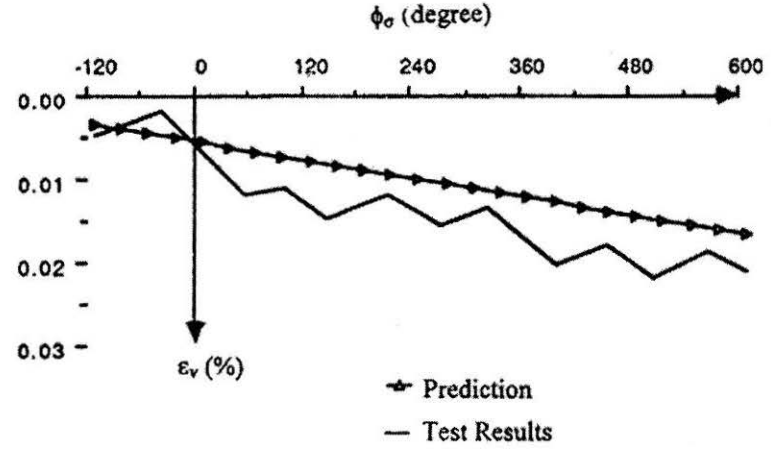

(d)

FIGURE 7 : Continued

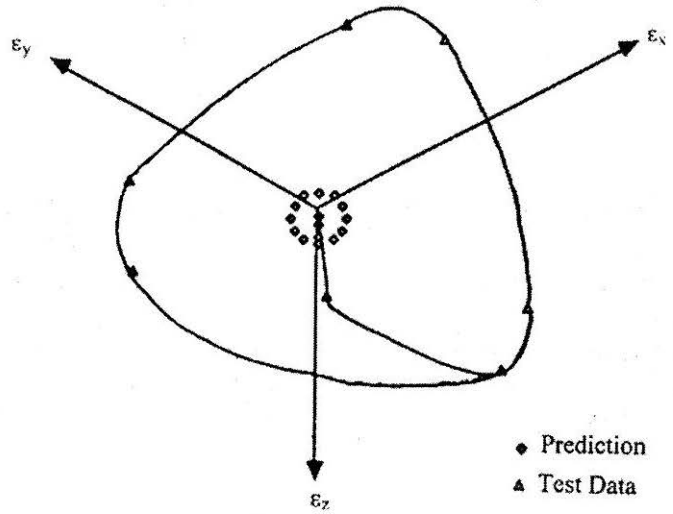

FIGURE 8 : Prediction for the Cubical Test along Circular Stress Path (in Strain p-Plane)

E, and bulk modulus, K, were obtained from a single triaxial consolidated drained compression test performed at a confining pressure of 245 kPa. The following functional forms for Young's modulus and bulk modulus were found to represent the elastic behaviour of the material reasonably well:

$$E = 62978.617 + 199.071\sigma_1 \tag{34}$$

$$K = 44660.0 \times 10^{0.0006726\sigma_3} \tag{35}$$

where, σ_3 is the confining pressure.

For the cemented sand, the

$$f_H = (1-\varphi_1)\varphi_0 + \varphi_1\sigma \tag{36}$$

The hydrostatic material parameter φ_0 was found to be a function of the confining pressure, σ_3 and well represented by the following expression:

$$\varphi_0 = 1200 - 1716 \cdot e^{-0.00889\sigma_3} \tag{37}$$

Unlike Hostun sand, in cemented sand the shear-volume relationship is found to be dependent on the initial confining pressures at which the tests

TABLE 3 : Material Parameters for Cemented Sand.

Elastic Parameters		
Bulk Modulus,	K (kPa)	$44660.0\times10^{0.0006726\sigma_3}$
Young's Modulus	E (kPa)	$62978.617+199.071\sigma_3$
Dilatancy Parameters	K	0.4225
	Γ_0	$0.99-0.492e^{-0.009423\sigma_3}$
Deviatoric Hardening Parameters	η	0.0016
	δ_0	0.114
Hydrostatic Hardening Parameters	φ_1	0.80
	φ_0	$1200-1716e^{-0.00889\sigma_3}$
	ϕ_0	1750000.0
Deviatoric Internal Variables	A_1	2300.0
	α_1	33.84
	A_2	300000.0
	α_2	803.233
	A_3	2450000.0
	α_3	7000.0

were conducted. The coupling of shear and volumetric parts remains indifferent to the confining pressure (k = constant), only the parameter Γ_0 varies depending upon the confining pressure. Thus the stress level at which the material starts to dilate shifts depending upon the confining pressure. The following functional form for Γ_0 has been found to work well for the cemented sand:

$$\Gamma_0 = 0.99-0.492e^{-0.009423\sigma_3} \tag{38}$$

The other material parameters were determined from the conventional triaxial compression test results performed at a confining pressure of 245 kPa. Table 3 shows all the material parameters for the cemented sand. The detail procedure for the determination of material parameters for the cemented sand is given in Sengupta and Saxena (1991).

Figures 9, 10 and 11 show the performance of the model for the case of cemented sand. Figure 9 compares the model predictions with the corresponding test results for a conventional triaxial compression test performed at a confining pressure of 49 kPa. Figure 10 shows the model

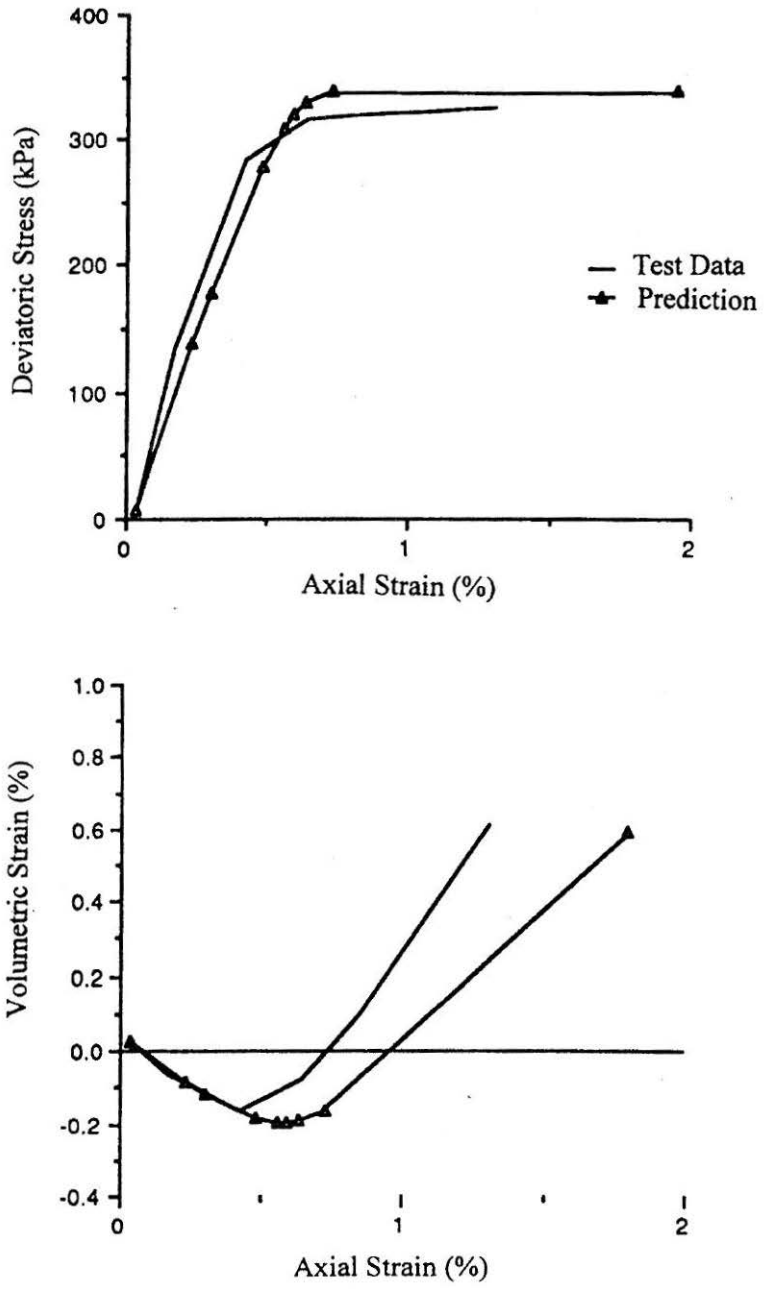

FIGURE 9 : Prediction for Cemented Sand (Consolidated Drained Triaxial Test at 49 kPa)

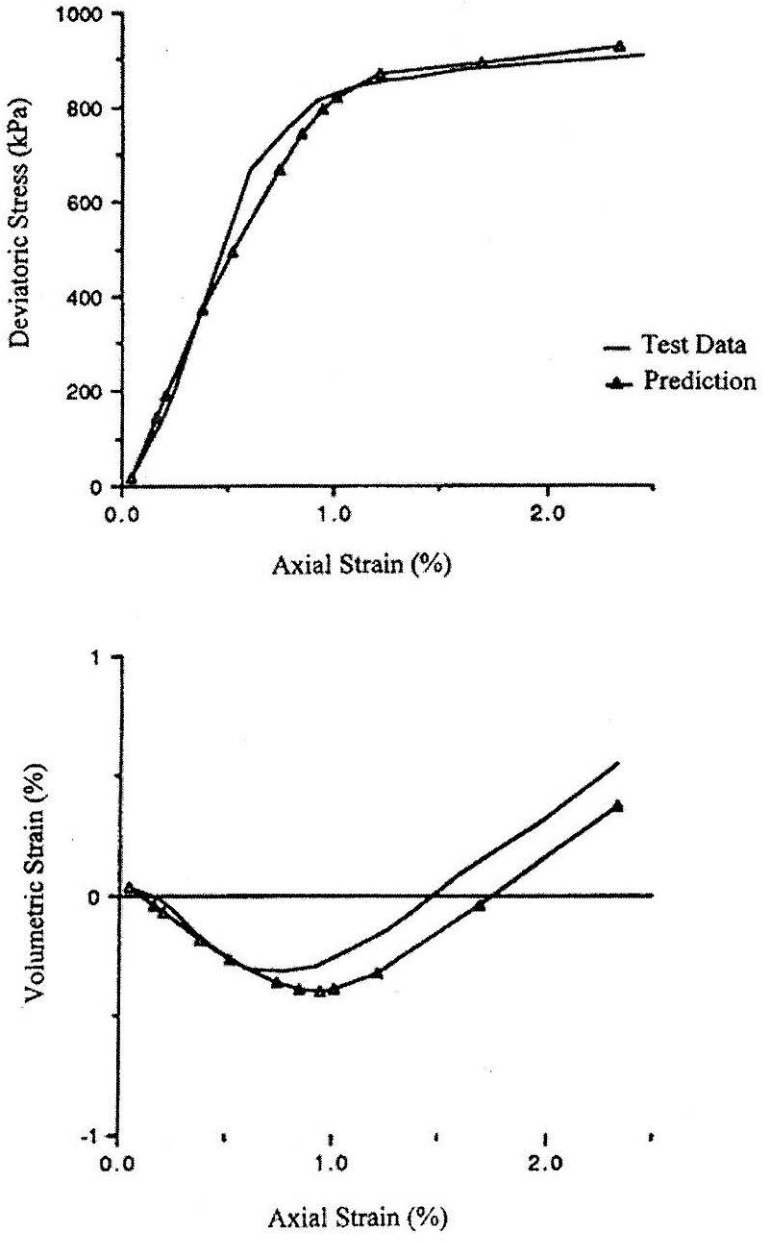

FIGURE 10 : Prediction for Cemented Sand (Consolidated Drained Triaxial Test at 245 kPa)

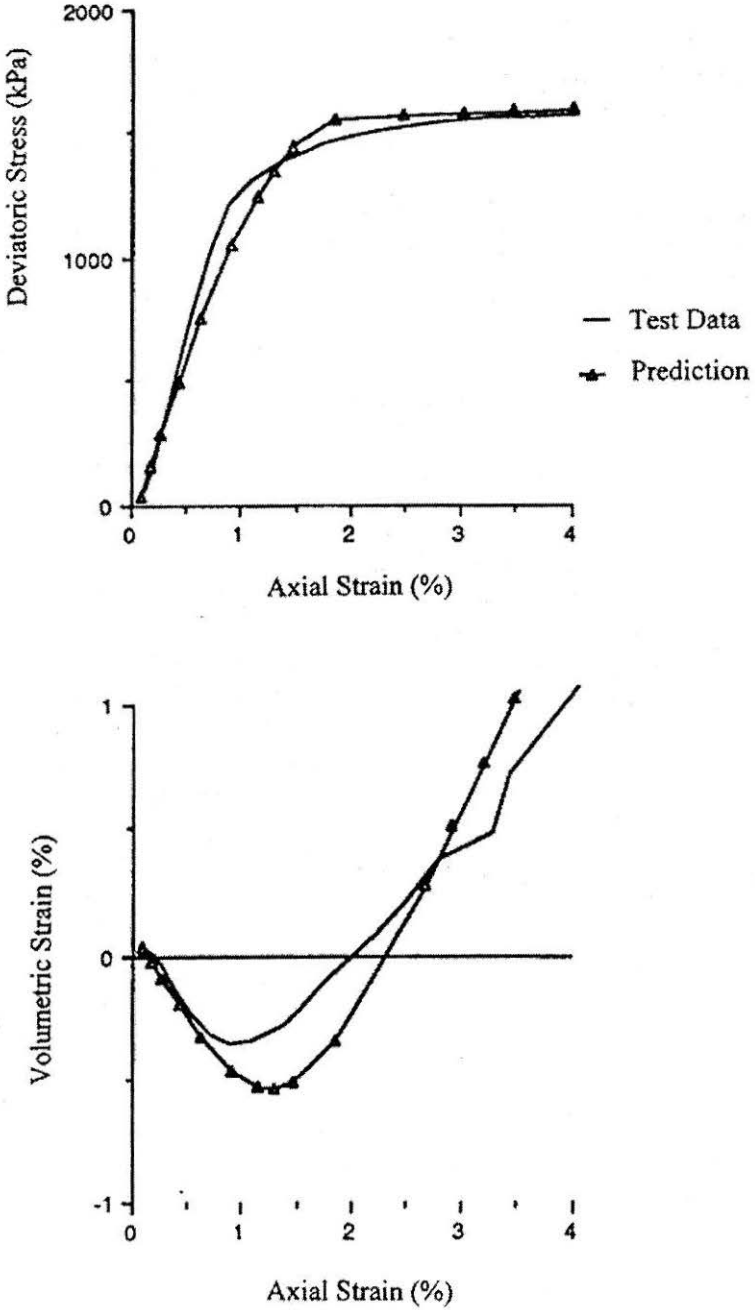

FIGURE 11 : Prediction for Cemented Sand (Consolidated Drained Triaxial Test at 490 kPa)

performance for a conventional triaxial compression test performed at a confining pressure of 245 kPa. Figure 11 compares the model predictions with the test results for a conventional triaxial compression test performed at a confining pressure of 490 kPa. The deviatoric stresses and volumetric strains predicted by the model with the progress of the loading were found to be very much comparable to the actual test results for all the cases. The relative density (DR) of the cemented sand was 80%. So it behaved like a dense soil. That is, it initially densified (contracted) a little bit and then exhibited dilative behavior. This change in volumetric strains from negative to positive values is very accurately duplicated by the thermodynamic model. Thus it may be concluded that the present thermodynamic model is capable of modeling stress dependency and shear dilatancy behaviours exhibited by dilatant soils, like, cemented sand.

Conclusions

The thermodynamics based theory for frictional materials has been found to be capable of predicting mechanical behaviour of a sand and a cemented sand quite well under conventional and non-conventional laboratory simulated stress paths for which the model was not calibrated. The present thermodynamic model is fully capable of modeling stress dependency and shear dilatancy behaviours exhibited by dilatant soils, like, dense sand and cemented sand.

The model has been found to be able to degenerate to a Mohr-Coulomb type of elastic-plastic theory showing prominent yield surfaces. The volume changes predicted by the model have been quite reasonable. Though the model requires quite a number of parameters, but these parameters have physical meaning and they can be determined from conventional triaxial and hydrostatic test results.

The model predictions for the case of Hostun sand are in general stiff as compared to the actual laboratory test results. The particular hollow cylinder test results used for the determination and calibration of model parameters are themselves stiffer as compared to other test results.

The model performances for the cyclic torsional and circular stress paths have not been that good due to the fact that the model in its present state does not include the effects of the third invariant of stresses. At present, research is underway to find a way to include the third invariant of deviatoric stresses into the formulation through the deviatoric hardening parameters of the thermodynamic model.

References

ARULANANDAN, K. and SCOTT, R.F. (eds.) (1993) : "Verification of Numerical Procedures for the Analysis of Soil Liquefaction Problems", *Proc. Intl. Conf. on the Verification of Numerical Procedures for the Analysis of Soil Liquefaction Problems*, Vol.I and II.

AVRAMIDIS, A. and SAXENA, S.K. (1985) : "Behaviour of Cemented-Stabilized Sands under Static and Dynamic Loads, Parts I and II", *Report No. IIT-CE-85-01*, Dept. of Civil Engg., IIT, Chicago.

DAFALIAS, Y.F. (1983) : "Plasticity Today", *Symp. on Recent Trends and Results in Plasticity*, Udine, 135-151.

DESAI, C.S., GALAGODA, H.M. and WATHUGALA, G.W. (1987) : "Hierarchical Modeling for Geologic Materials and Discontinuities –Joint Interfaces", *Proc. of 2nd Intl. Conf. on Constitutive Laws for Engg. Matl. – Theory and Applications* (eds. C.S. Desai, E. Krempl, P.D. Kiousis and T. Kundu), 1, 81-94.

DRUCKER, D.C. (1956) : "A Definition of Stable Inelastic Material", *J. Appl. Mech.*, 26, 101-106.

DRUCKER, D.C. (1956) : "On Uniqueness in the Theory of Plasticity", *Quarterly Appl. Math.*, 14, 35-42.

DUNCAN, J.M. and CHANG, C.Y. (1970) : "Nonlinear Analysis of Stress and Strains in Soils", *J. Soil Mech. & Found. Div.*, ASCE, 96, SM5, 1629-1653.

LADE, P.V. (1977) : "Elasto Plastic Stress-Strain Theory for Cohesionless Soil with Curved Yield Surfaces", *Intl. J. Solids and Structures*, 13, 1019-1035.

LADE, P.V., Nelson, R.B. and ITO, Y.M. (1987) : "Nonassociated Flow and Stability of Granular Materials", *J. Engrg. Mech.*, ASCE, 113, 9, 1302-1318.

MANDEL, J. (1964) : "Conditions de Stabilite et Postulat de Drucker", *Proc. Intl. Union Theoretical Appl. Mech. Symp. on Rheology and Soil Mech.*, Grenoble, France, 58-67.

MROZ, Z. and ZIENKIEWICZ, O.C. (1984) : "Uniform Formulation of Constitutive Equations for Clays and Sands", *Mech. of Engg. Matl.* (eds. C.S. Desai and R.H. Gallagher), 415-449.

PREVOST, J.H. (1978) : "Plasticity Theory for Soil Stress-Strain Behaviour", *J. of Eng. Mech. Div.*, ASCE, 104, EM5.

ROSCOE, K.H. and BURLAND, J.B. (1968) : "On the Generalized Stress-Strain Behaviour of 'Wet' Clays", *Engineering Plasticity* (eds. J. Heyman and F.A. Lackie), Cambridge University Press.

SAADA, A.S. (ed.) (1987) : "Test Results and Predictions" *Intl. Workshop on Constitutive Equations for Granular Non-Cohesive Soils*, Case Western Reserve Univ..

SANDLER, I.S., DiMAGGIO, F.L. and BALADI, G.Y. (1976) : "Generalized Cap Model for Geological Materials", *J. of Geotech. Engg. Div.*, ASCE, GT7.

SENGUPTA, A. and SAXENA, S.K. (1989) : "Application of a Thermodynamic Theory to Soils and Concrete", *Report to U.S. Army Engineers Waterways*

Experiment Station, Vicksburg, Report No. IIT-CE-89-01, Mississippi.

SENGUPTA, A. and SAXENA, S.K. (1991) : "Review of a Thermodynamic Theory for Granular Materials", *Computers and Geotechnics*, 11, 1-36.

VALANIS, K.C. and PETERS, J.F. (1988) : "Thermodynamics of Frictional Materials", *Report I - A Constitutive Theory of Soil with Dilatant Capability*, U.S. Army Corps of Engineers, Waterways Experiment Station, Vicksburg.

YONG, R.K. and KO, H.Y. (eds.) (1980) : *Limit Equilibrium, Plasticity and Generalized Stress-Strain in Geotechnical Engineering*, McGill University.

Notations

α_r = Deviatoric Internal Variables.

β_r = Hydrostatic Internal Variables.

Φ_s = Stress Phase Angle.

Γ_o = Material Parameter.

δ_{ij} = Dirac-Delta Function.

δ_o = Material Constant.

ε_x, ε_y, ε_z = Total Strains in x, y and z directions.

ε^P = Hydrostatic Plastic Strain.

ϕ = Friction Angle.

$\phi_o = \sum_{r=1}^{N} B_r$

γ = Unit Weight of a Material.

η = Material Constant.

φ_o = Material Constant.

φ_1 = Material Constant.

$\rho_o = \sum_{r=1}^{N} A_r$

σ = Mean Stress $(=\frac{\sigma_{kk}}{3})$

σ_1, σ_2, σ_3 = Principal Stresses.

σ_x, σ_y, σ_z = Stresses in x, y and z directions.

σ_Y = Yield Stress.

σ_{kk} = Volumetric Stress.

A_r = Deviatoric Internal Variables.

B_r = Hydrostatic Internal Variables.

b = Stress Ratio.

$b_{21}^{(r)}$ = Resistance Tensor.

E = Young's Modulus.

$\tilde{e}^P$ = Deviatoric Plastic Strains.

f_D = Deviatoric Hardening Function.

f_H = Hydrostatic Hardening Function.

G = Shear Modulus.

K = Bulk Modulus.

k = Coupling Constant.

$\tilde{s}$ = Deviatoric Stress Tensor.

Z = Intrinsic Time Scale.

Z_D = Deviatoric Component of Intrinsic Time Scale.

Z_H = Hydrostatic Component of Intrinsic Time Scale.